Impact of Antenna Configuration and Shadowing on the Characteristics of the 60 GHz Indoor Wideband Radio Channel

Michael Peter, Wilhelm Keusgen

Fraunhofer-Institut für Nachrichtentechnik, Heinrich-Hertz-Institut, Einsteinufer 37, 10587 Berlin, Germany
Phone: +49 30 31002-{583, 639}, e-mail: {michael.peter, wilhelm.keusgen}@hhi.fraunhofer.de

Abstract

In this paper, we present the results of an extensive measurement campaign concerning the 60 GHz indoor wideband radio channel. Three different antenna configurations are considered involving omnidirectional and directional antennas. We analyze the impact of the antenna configuration on the time dispersion and the normalized received power under line-of-sight (LOS) as well as under obstructed line-of-sight (OLOS) conditions.

1. Introduction

The growing demand for wireless broadband multimedia services gives rise to high requirements on systems for short-range radio data transmission and bears a considerable technical challenge [1]. Since future usage scenarios call for wireless systems with an aggregate capacity of up to several Gbit/s, great efforts are currently made with regard to new concepts and standards. A promising approach to achieve rates beyond 1 Gbit/s is the utilization of unused frequency resources within the millimeter wave band. The IEEE 802.15.3 Task Group 3c (TG3c) is working towards an alternative physical layer (PHY) for the 802.15.3 Wireless Personal Area Network (WPAN) standard. The systems are supposed to operate in the unlicensed band from 57 to 64 GHz and are a candidate for indoor and in-vehicular [2] high speed internet access as well as real-time video streaming. To provide a basis for system design and implementation, it is essential to characterize millimeter wave propagation in application-oriented environments [3]. We performed wideband channel measurements in a conference room to investigate the influence of the antenna configuration and shadowing on the characteristics of the 60 GHz indoor radio channel. The paper gives an overview over the measurement campaign and the investigations concerning the received power and the time dispersion of the channel.

2. Indoor Broadband Channel Measurements

The measurements were performed in a conference room located on the ground floor of the institute building. We used a measurement setup based on pulse compression covering a bandwidth of 1 GHz around the center frequency of 61 GHz. The system allows for taking snapshots of the channel impulse response (CIR) with an adjustable rate. Each measurement yields a coherent set of CIRs. More details of the setup can be found in [4]. Fig. 1 shows the floor plan of the separable conference room. The partition wall was closed, so that the room size was approximately 6.6 m $\times$ 5.9 m. The room is provided with four windows integrated in the ceiling and a glass door towards the corridor. It was furnished with tables and chairs. The location of the transmitter (Tx), representing the access point, was fixed, whereas the receiver (Rx) was considered as a mobile terminal and placed at twelve different locations around the tables according to Fig. 1. For each Rx location (Rx loc.) and each antenna configuration a spatial small-scale measurement set of 100 CIRs has been acquired. Three different antenna configurations have been considered: omnidirectional antennas at the Tx and the Rx (OO), an omnidirectional antenna at the Tx and a Vivaldi antenna at the Rx (OV) and Vivaldi antennas at both the Tx and the Rx (VV). The omnidirectional antennas have an almost constant pattern in the azimuth plane and an FWHM (full width at half maximum) of about $\Theta_{3\mathrm{dB}} = 70^\circ$ in elevation. This results in a maximum gain of 2 dBi. The Vivaldi antennas are directional antennas with a gain of approximately 12 dBi and an FWHM of $\Theta_{3\mathrm{dB}} = 33^\circ$ in both azimuth and elevation plane. All antennas were vertically polarized. The stationary Tx antenna was mounted at a height of 245 cm with a downtilt of 15°. Since the transmitter should represent a fixed access point, the antenna was not

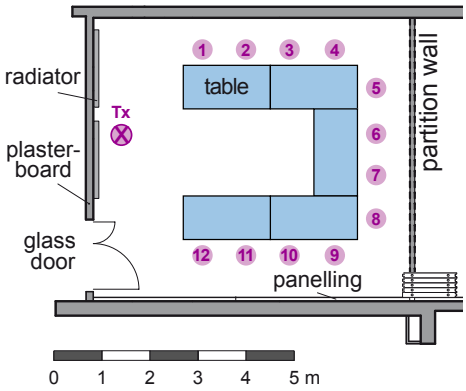

Fig. 1: Floor plan of the conference room, numbered circles mark the Rx locations.

moved or adjusted during the measurement, whereas the Rx antenna had always been aligned towards the Tx antenna in the horizontal plane. In order to be able to remove the effects of spatial small-scale fading, the Rx antenna (mounted at a height of 130 cm) was moved on a linear track over a distance of 10 cm by the help of a controllable positioning platform. This results in a spatial separation of 1 mm between two consecutive snapshots. LOS and OLOS conditions have been considered. OLOS was realized by blocking the line-of-sight between Tx antenna and Rx antenna with an absorber mat of size 60×60 cm. Additional measurements were performed to investigate the effects of temporary shadowing by a human body. The acquired data set comprises more than 10,000 complex-valued CIRs.

3. Normalized Received Power

The normalized received power (NRP) $P_{R,\mathrm{norm}}$ was calculated on the basis of the averaged power delay profiles (APDPs). An APDP is given by

$$\overline{p}(\tilde{\tau}) = \frac{1}{K}\sum_{k=1}^{K} p_k(\tilde{\tau}) = \frac{1}{K}\sum_{k=1}^{K} |h_{b,k}(\tilde{\tau})|^2, \qquad (1)$$

where $\tilde{\tau}$ is the delay, $p_k(\tilde{\tau})$ denotes the individual power delay profile (PDP) of channel observation (snaphot) k at a particular Rx location, and $h_{b,k}(\tilde{\tau})$ is the corresponding bandlimited CIR. $P_{R,\mathrm{norm}}$ can be calculated by integrating all multipath power above the noise floor:

$$P_{R,\mathrm{norm}} = \int_{\tilde{\tau}_0}^{\tilde{\tau}_{\max}} \overline{p}(\tilde{\tau})\, d\tilde{\tau}, \qquad (2)$$

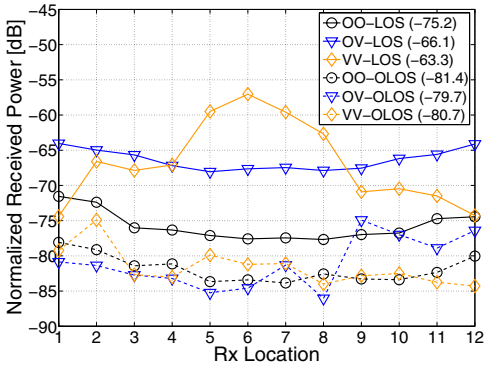

Fig. 2: NRP versus Rx loc., average values (dB) are given in brackets.

where $\tilde{\tau}_0$ and $\tilde{\tau}_{\max}$ were determined by applying a threshold of -30 dB with respect to the strongest component, resulting in a maximum value of approx. 125 ns for $\tilde{\tau}_{\max}$. Fig. 2 illustrates $P_{R,\mathrm{norm}}$ at the 12 Rx locations for all antenna configurations. Under LOS conditions (solid lines), the power is expected to decay when the Tx-Rx distance is increased and vice versa. This is true for the OO and the OV config. (see Fig. 1), but it is not the case for the VV config. The received power is smallest for the nearby locations and reaches its maximum at loc. 6, which is 4.6 m away from the transmitter. This effect becomes clear, when we bear in mind that the mounting height of the Tx antenna was 1.15 m above the height of the Rx antenna, and the Tx antenna pointed towards the back wall of the room. As a result, the alignment was poor for the nearby locations. At most of the Rx loc. the NRP is around 10 dB higher for the OV configuration with respect to the OO configuration. This is in accordance to the expected value due to the antenna gain of the Vivaldi antenna compared to the omnidirectional one. An additional gain of 10 dB can be achieved with the VV configuration, but only for Rx loc. 6. For seven of the twelve Rx loc. the NRP is smaller than for the OV case.

In general, millimeter wave systems are proposed for LOS transmission, but in practical scenarios intervisibility between Tx and Rx antenna might not be guaranteed. To investigate the impact of an obstructed line-of-sight, the measurement procedure was carried out twice for each Rx loc. During the second measurement, the LOS was blocked by an absorber mat. One would expect that the OO configuration performs best under OLOS conditions since multipath power can be collected from all directions. However, the measurement results did not comply with this expectation. The average OLOS values of $P_{R,\mathrm{norm}}$ (dashed lines) are almost identical, and the curves in Fig. 2 are quite close to each other. By inspecting the APDPs we could ensure that the (virtual) LOS-MPC did not penetrate the absorber mat. Indeed, there are MPCs whose powers sum up to values corresponding to an NRP of around -80 dB.

4. Temporary Shadowing

In order to further investigate the influence of an obstructed LOS, additional measurements were performed with temporary shadowing. Fig. 3 gives a vivid impression of the typical effects of shadowing by the absorber mat and a person crossing the LOS. In the shown example, the power of the first resolvable component (LOS-RMPC) drops about 32.2 dB. The loss in total power is 23.8 dB. We see that the impact of human shadowing is significantly less severe than effects caused by the absorber mat. The loss of total power is around 7.0 dB. Values up to 13 dB have been observed for other Rx locations. In contrast, values up to 5 dB arose for the OO configuration, but one must

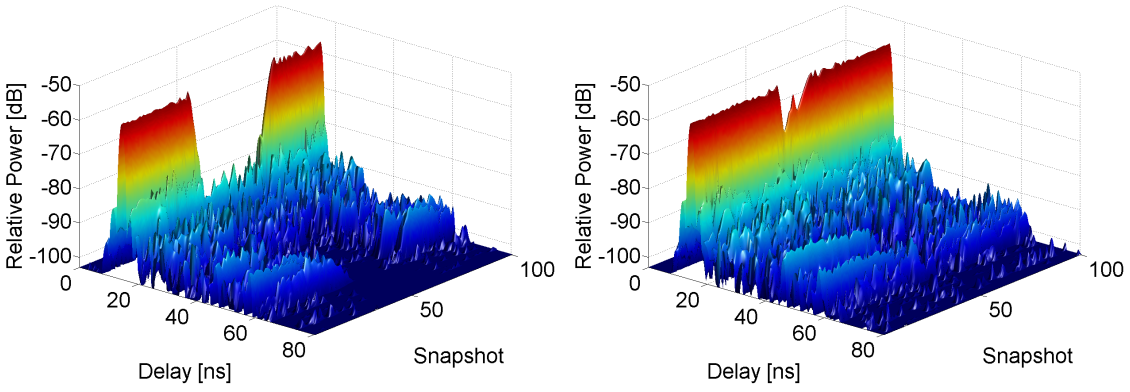

(a) Absorber (b) Human body

Fig. 3: Effects caused by temporary shadowing for the VV configuration at Rx loc. 6.

bear in mind that the reference (received LOS power) is much lower in this case. Frequently, OLOS measurement results are derived from the LOS CIRs by mathematical removal of the "direct ray" (LOS-MPC). Since MPCs cannot be resolved in general, this is only possible within the temporal resolution. In fact, not the distinct LOS-MPC but the LOS-RMPC is removed. Therefore, in [5] it is stated that this is a somewhat pessimistic approach since some part of the diffracted rays is removed, too. However, in realistic obstruction scenarios, not only the LOS-MPC might be eliminated, but also other MPCs arising from similar angles of departure or angles of arrival – depending on whether the obstructing object is situated nearby the Tx or the Rx antenna. This effect is clearly visible in Fig. 3. Consequently, the approach can also be too optimistic. The actual impact of shadowing strongly depends on the size, the material and the position of the obstructor as well as on the directivity of the antennas. Hence, one should carefully analyze if the "mathematical approach" for OLOS is adequate under the investigated conditions. The minimum power within the measurement set with human body shadowing is reached after three snapshot intervals corresponding to 150 ms, whereby the person crossed the line-of-sight with a speed of approximately $0.4\ \frac{\mathrm{m}}{\mathrm{s}}$. Assuming a maximum speed of $2.0\ \frac{\mathrm{m}}{\mathrm{s}}$, severe fluctuations of the channel state due to human body shadowing can occur within an interval of 30 ms.

5. Time Dispersion

Several publications deal with the time dispersion of the 60 GHz indoor channel. In [6] the channel has been measured by means of highly directional antennas, whereas in [7] omnidirectional antennas have been used. In [8] the influence of different antenna types is also investigated. In order to characterize the time dispersion of the channel, we derived the RMS delay spread from the APDPs for each antenna configuration and each Rx location:

$$\overline{\tau}_{\mathrm{rms}} = \sqrt{\frac{\int_0^{\overline{\tau}_{\max}} \tau^2 \cdot \overline{p}(\tau)\, d\tau}{\int_0^{\overline{\tau}_{\max}} \overline{p}(\tau)\, d\tau} - \overline{\tau}_{\mathrm{m}}^2} \tag{3}$$

with

$$\overline{\tau}_{\mathrm{m}} = \frac{\int_0^{\overline{\tau}_{\max}} \tau \cdot \overline{p}(\tau)\, d\tau}{\int_0^{\overline{\tau}_{\max}} \overline{p}(\tau)\, d\tau}, \tag{4}$$

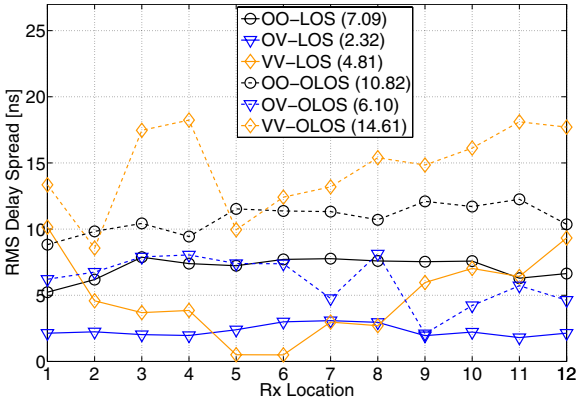

Fig. 4: RMS delay spread for different antenna configurations, average values (ns) are given in brackets.

where $\tau = \tilde{\tau} - \tilde{\tau}_0$, $\overline{\tau}_{\mathrm{m}}$ and $\overline{\tau}_{\max}$ denote the excess delay, the mean excess delay and the maximum excess delay, respectively. Again, a threshold of -30 dB relative to the strongest component was used to determine $\tilde{\tau}_0$ and $\overline{\tau}_{\max} = \tilde{\tau}_{\max} - \tilde{\tau}_0$. Fig. 4 shows the delay spread with respect to the Rx loc. 1–12 (see Fig. 1) for all considered antenna combinations. Solid lines refer to the LOS cases, dashed lines to OLOS conditions. The average RMS delay spread values are also given in Fig. 4. Comparing the LOS results, we see that the curves are quite flat for the OO and the OV configuration, which means that the RMS delay spread is only weakly related to the actual Rx loc. or

the distance between Tx and Rx. The values are 5.2–7.9 ns (OO) and 1.8–3.1 ns (OV), respectively. Applying the directional antenna at the Rx side reduces $\overline{\tau}_{\mathrm{rms}}$ to approximately one third on average in LOS scenarios – compared to the OO configuration. The VV curve shows a completely different behavior. The largest delay spread (10.2 ns) is observed at Rx loc. 1, whereas the lowest values of 0.5 ns (equivalent to the RMS delay spread of the sounding pulse) arises at loc. 5 and 6. Again, the impact of the antenna pointing error emerges. The transition from LOS to OLOS increases the mean delay spread significantly in all cases. The increase is around 50% for the OO, 160% for the OV and 204% for the VV configuration. While the OV value remains below the delay spread of the OO case, even compared to the LOS value, the average $\overline{\tau}_{\mathrm{rms}}$ of the VV configuation exceeds the OO value by 35%.

6. Conclusion

In this paper, we presented major results of a measurement campaign regarding the 60 GHz indoor channel. Three different antenna configurations have been investigated. As stated in [8], the patterns of the antennas have a great impact on the time dispersion of the channel. Under LOS conditions, the average RMS delay spread reduces to one third by applying a directional antenna with a gain of 12 dBi at the Rx side (OV). If at most one directive antenna is used, the variance of $\overline{\tau}_{\mathrm{rms}}$ is small with respect to different Rx locations. The delay spread can be decreased further by additionally using a directional antenna at the transmitter (VV), but only for a good alignment – which might not be guaranteed under realistic conditions. Obstructing the LOS significantly increases the delay spread. The VV configuration yields the largest values in the OLOS case. Under LOS conditions the received power reaches its maximum for the VV configuration, but the theoretical gain of 20 dB – compared to the OO configuration – is only achieved for a single Rx loc. In contrast, a gain of approximately 10 dB is achieved in the OV case for almost all Rx locations. Counter-intuitively, the average NRP is almost identical under OLOS conditions for all antenna combinations. This result might depend on the scenario, but we conclude that an OO configuration does not outperform configurations with moderately directive antennas in general. However, if a system with directive antennas is supposed to sustain a link even under OLOS conditions, it must not rely on the large received LOS power, but it must be capable to switch to another mode that allows for data transmission with a 20 dB lower SNR. In contrast, the gap between average LOS and OLOS received power is only around 6 dB for the OO case, and the fluctuations of power are much smaller with respect to the actual Rx loc. In any case, a high-rate millimeter wave wireless system is to be highly adaptive to the channel conditions and should involve mechanisms like macroscopic diversity in order to ensure a reliable transmission.

7. References

[1] P. Smulders. Exploiting the 60 GHz band for local wireless multimedia access: prospects and future directions. *Communications Magazine, IEEE*, 40(1):140–147, 2002.

[2] M. Peter, W. Keusgen, and M. Schirrmacher. Measurement and analysis of the 60 GHz in-vehicular broadband radio channel. In *Vehicular Technology Conference, 2007. VTC 2007-Fall. 2007 IEEE 66th*, Sept.–Oct. 2007.

[3] P. F. M. Smulders and L. M. Correia. Characterisation of propagation in 60 GHz radio channels. *Electronics & Communication Engineering Journal*, 9(2):73–80, 1997.

[4] M. Peter and W. Keusgen. A component-based time domain wideband channel sounder and measurement results for the 60 GHz in-cabin radio channel. In *Antennas and Propagation, EuCAP 2007. The second European Conference on*, Nov. 2007.

[5] P. F. M. Smulders. *Broadband Wireless LANs: A Feasibility Study*. PhD thesis, Eindhoven University of Technology, The Netherlands, 1995.

[6] R. Davies, M. Bensebti, M. A. Beach, and J. P. McGeehan. Wireless propagation measurements in indoor multipath environments at 1.7 GHz and 60 GHz for small cell systems. In *Vehicular Technology Conference, 1991. 'Gateway to the Future Technology in Motion', 41st IEEE*, pages 589–593, 1991.

[7] T. Zwick, T. J. Beukema, and H. Nam. Wideband channel sounder with measurements and model for the 60 GHz indoor radio channel. *Vehicular Technology, IEEE Transactions on*, 54(4):1266–1277, 2005.

[8] T. Manabe, Y. Miura, and T. Ihara. Effects of antenna directivity and polarization on indoor multipath propagation characteristics at 60 GHz. *Selected Areas in Communications, IEEE Journal on*, 14(3):441–448, 1996.